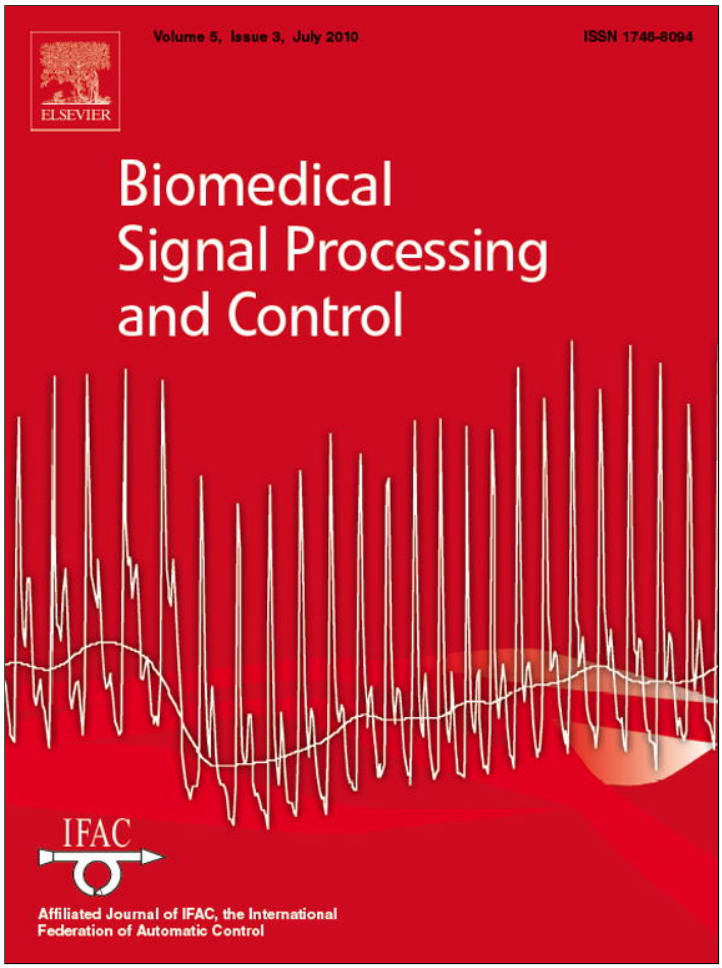

Biomedical Signal Processing and Control 5 (2010) 223–228

Contents lists available at ScienceDirect

Biomedical Signal Processing and Control

journal homepage: www.elsevier.com/locate/bspc

Technical note

Software controlling algorithms for the system performance optimization of confocal laser scanning microscope

Shuo Chen[a], Xiaorui Feng[a], Yiming Li[a], Chuanqing Zhou[a], Peng Xi[a,b,*], Qiushi Ren[a,b,*]

[a] Department of Biomedical Engineering, School of Life Sciences and Biotechnology, Shanghai Jiao Tong University, No. 800 Dongchuan Road, Shanghai 200240, PR China
[b] Department of Biomedical Engineering, College of Engineering, Peking University, No. 5 Yiheyuan Road, Beijing 100871, PR China

ARTICLE INFO

Article history:
Received 14 December 2009
Received in revised form 26 February 2010
Accepted 12 March 2010
Available online 18 April 2010

Keywords:
Confocal
Laser scanning
Data acquisition
Image reconstruction

ABSTRACT

The relative slow scanning speed of a galvanometer commonly used in a confocal laser scanning microscopy system can dramatically limit the system performance in scanning speed and image quality, if the data collection is simply synchronized with the galvanometric scanning. Several algorithms for the optimization of the galvanometric CLSM system performance are discussed in this work, with various hardware controlling techniques for the image distortion correction such as pixel delay and interlace line switching; increasing signal-to-noise ratio with data binning; or enhancing the imaging speed with region of interest imaging. Moreover, the pixel number can be effectively increased with Acquire-On-Fly scan, which can be used for the imaging of a large field-of-view with a high resolution.

1. Introduction

Confocal microscopy has been served as a very important tool for biological cellular imaging. In order to obtain the 3D biological contrast, the relative movement between the focal spot and the sample is essential in confocal laser scanning microscopy (CLSM). Laser scanning has been widely employed in confocal imaging as it can provide a much faster scanning speed for lateral imaging than mechanical scan methods [1]. There are many laser scanning methods in CLSM, e. g. galvanometric scan, resonant scan, polygon mirror, slit scan, and Nipkow disk etc. [2]. Among them, the 2D galvanometric scan is still the most popular scanning scheme as it provides a compromise between frame rate and image quality [3].

Although many commercial confocal systems provide various types of confocal units to meet the needs of biological imaging, a complete customized confocal system can serve for a specific imaging project and is often more cost effective [4–6]. As a very important advance of CLSM, multiphoton microscopy (MPM) has been widely used in neuron imaging as it provides a much deeper penetration depth [7–9]. Several groups have already developed their own MPM based on the adaption of an ultrashort pulsed laser onto a custom-built or commercial confocal microscope [10–16].

Currently, as most hardware components of CLSM (optics, scanning mirrors, detectors and computers) are commercially available, the largest hurdle lies on the software development to control the scanning unit, to reconstruct the confocal image and to optimize the performance of the confocal system [4,17]. Although various versions of software programmed in Matlab, LabVIEW, VB Script, etc. are freely available, the major focus on these programs are the raster scan of CLSM and the reconstruction of the confocal image [4–6]. The most straightforward way to control the galvanometer is that a (X,Y) position is sent to the galvanometer, usually in a raster mode, and the image intensity data is read from the detector simultaneously [5,6,17]. The performance of the laser scanning system can be improved if the movement feature of the galvanometric scanning unit and the speed difference between the scanning and digitization (data collection) are considered. In this work we examined the limitation of the galvanometric scanning confocal system, and several modes in scan control, sampling, as well as image reconstruction are optimized for the efficient use of the hardwares. Image distortion due to the mechanical galvanometric movement can be compensated with pixel delay, as well as interlace line switch in bi-direction scan. The signal-to-noise ratio (SNR) can be improved with data binning. The imaging speed can be increased when scanning a small region of interest (ROI) instead of the whole field-of-view (FOV). With the Acquire-On-Fly (AOF) scan the pixel number can be effectively increased. Thus, in cases that the resolution is limited by the sampling pixel numbers (for large FOV imaging), this method can be utilized to increase the resolution. As the proposed problems commonly exist in most galvanometric scanning system, the

* Corresponding authors at: Department of Biomedical Engineering, College of Engineering, Peking University, No. 5 Yiheyuan Road, Beijing 100871, PR China.
E-mail addresses: xipeng@coe.pku.edu.cn (P. Xi), renqsh@coe.pku.edu.cn (Q. Ren).

1746-8094/$ – see front matter © 2010 Elsevier Ltd. All rights reserved.
doi:10.1016/j.bspc.2010.03.002

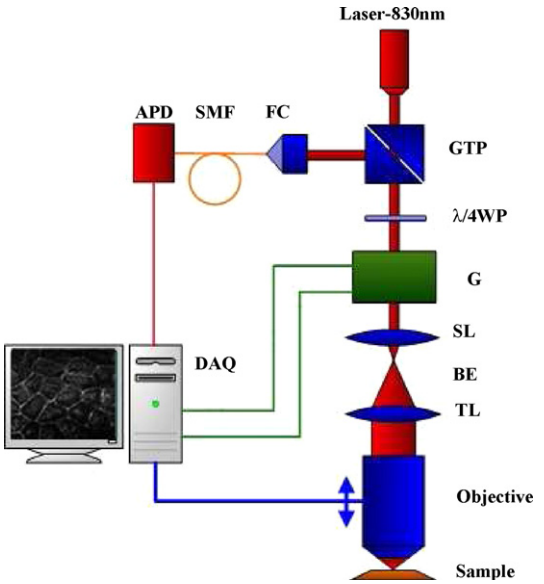

Fig. 1. Diagram of the CLSM used in this work. LD: Laser diode; GTP: Glenn–Taylor prism; WP: wave plate; FC: fiber collimator; SMF: single mode fiber; APD: avalanche photodiode; G: galvanometer; BE: beam expansion; SL: scan lens; TL: tube lens.

methods can be applied to various types of galvanometric scanning systems.

2. Methods and materials

We have constructed a reflective confocal laser scanning microscope used in this work. An 830 nm laser diode (Thorlabs, DL5032-001) was used. The s-polarization incident beam passed through Glan-Taylor prism (Daheng, GCL-070212) as well as a quarter-wave plate (Daheng, custom made), forming a circularly polarized light. The beam was scanned with a pair of galvanometer (Cambridge Technologies, 6215H). A 15× microscopic eyepiece (Nikon) was used as the scan lens to deliver the beam onto the objective. The light was scanned onto the sample through a Nikon Ti-U inverted microscope with a 40× oil-immersion Apo-chromatic objective (N.A. 1.3), and back-scattered light from the sample travelled onto the galvanometer and got de-scanned. When the reflected signal reached the quarter wave plate, the polarization degree shifted to p-polarization state. The prism then reflected the beam onto a fiber collimator (Thorlabs, F220FC-B) to guide the signal to the avalanche-photodiode (Hamamatsu C5460) through a single-mode fiber (Go4Fiber, S1-F2 F2-01-0020-GF). The 9 μm fiber core also plays the role of the confocal pinhole in the system [6,18]. The complete system diagram is shown in Fig. 1.

The scan signal generation and data acquisition hardware used in this work is similar to our previous work in [6,15,16]. In brief, National Instruments PCI-6251 is employed as the I/O board, which can provide 2 analog outputs at a speed of 2.8 MS/s and 16 channels of analog input (maximum speed of 1.25 MS/s).

Custom program is written with LabVIEW (National Instruments) and is designed for personal computers running under a Windows environment. The advantage of using LabVIEW as the programme language is that it provides a user-friendly graphic programming environment and fully compatible with the data acquisition (DAQ) board. This software is designed to generate the scan signal for the galvanometer and reconstruct the signal from the detector to an image. To facilitate the multi-channel signal detection, the parameters of individual channels can be set separately. The images are saved as TIF files, which can host 16-bit high dynamic range scientific images and can be analyzed in image processing software such as ImageJ (NIH). The graphic user interface (GUI) and flow chart of the software are shown in Fig. 2.

3. Results and discussion

3.1. Pixel delay

Because of the response time of the galvanometer, the user's commands cannot immediately generate a movement of the gal-

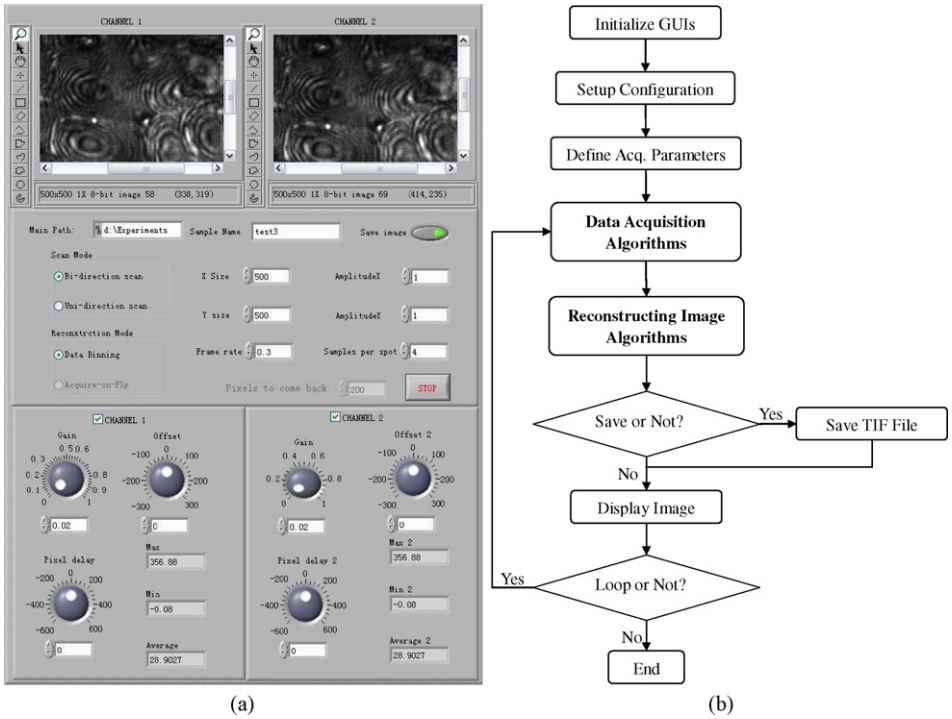

Fig. 2. The CLSM controlling program: (a) GUI and (b) the flow chart.

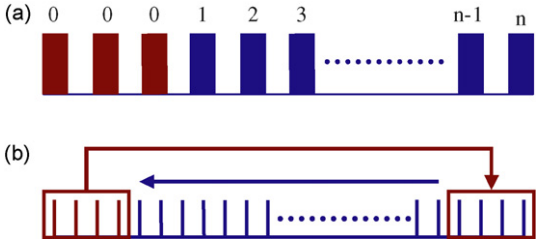

Fig. 3. Response delay of the galvanometer (a) and pixel shift correction method (b). The blue pixels are the ones that contain imaging data from the sample; and the brown pixels indicate the collection before the galvanometer responding and thus contain no information.

vanometer. Instead, the galvanometer has a fixed response delay if the data acquisition is at the same time of the scan command, which lead to the delay of acquiring data and the distortion of image during image reconstruction if this is not properly addressed. There exists several versions of ImageJ plug-ins, for example "Correct X Shift" by Krempp (http://rsbweb.nih.gov/ij/plugins/correct-shift.html) which shifts the X distortion by pixel on the odd lines so the image width gets smaller when shifted, and "X Shifter" by Xi (http://rsbweb.nih.gov/ij/plugins/x-shifter.html) which shifts the pixel to the following line so there are 2 pixel difference between the neighboring line on each pixel shift. These non-real time image processing tools can only be used to process the collected image, yet real time processing is of highly importance for the confocal user to visualize the structure of the sample properly.

The scheme of pixel shift is illustrated in Fig. 3. In our program, the image data was collected at the same time of scan commanding. To compensate for the response delay, a number of pixels at the front of data collection were rolled back to the end of the data, resulting in pixel delay of the image (Fig. 4). This corresponds to the delay of data acquisition of the DAQ board and realizes the synchronization of the galvanometer scan and data acquisition. The number of the pixel shift is dependent on the galvanometer hardware. In our system, a response delay of 326.8 μs is applied, which corresponds to 21 pixels for 256 × 256 image acquisition at 1 fps. It should be noted that due to the pixel shift, the last several pixels do not contain the real information in the first image. However, as most biological information locates at the central part, this does not create any noticeable effect to the image.

3.2. Interlace line switch

In bi-direction scan the galvanometer scans forward and then backward commanded at the same speed, and data were collected at both scan direction. The scan comanding scheme is shown in Fig. 5.

Unfortunately, one of the problems we found for the bi-direction scan is that, the speed of the forward scan and backward scan is not simply symmetric but attenuated by the acceleration of the galvanometric control due to the fast scan acceleration. This makes the line shift distortion presented in the image. To correct the line shift, the pixels in the even (back) line of the forward scan are switched with the odd (forward) scan line of the back scan, so that in each obtained image all the scan lines have the same scan direction, as illustrated in Fig. 6. A tri-stained mouse kidney sample were imaged with two-photon fluorescence excitation to demonstrate the effect of line switch (the experimental setup were described in [15,16]). It can be seen that when line switch is applied, the lectin wheat germ agglutin (stained with Alexa-488 and mapped to the green channel of the image) and the filamentous actin (stained with Alexa-568 and mapped to the red channel) in the mouse kidney glumeruli clearly showed their structures (Fig. 6d); whereas in the non-corrected image all theses structures are blurred (Fig. 6c). Naturally, the position of the blur are the same to all the three dyes, because of the same scanning direction when collecting the images of the three channels. An alternative way to cancel the blur is to shrink the image to its 25% of total size; by doing so all the odd (or even) lines are removed; however the pixel number is dramatically decreased, and that can affect either the resolution (if the initial image contains a proper sampling) or FOV (if the initial image is taken with 2× excessive sampling). Note that for uni-direction scan (Fig. 9a) the line shift is not presented, simply because the scan directions are constant for all the lines on the image.

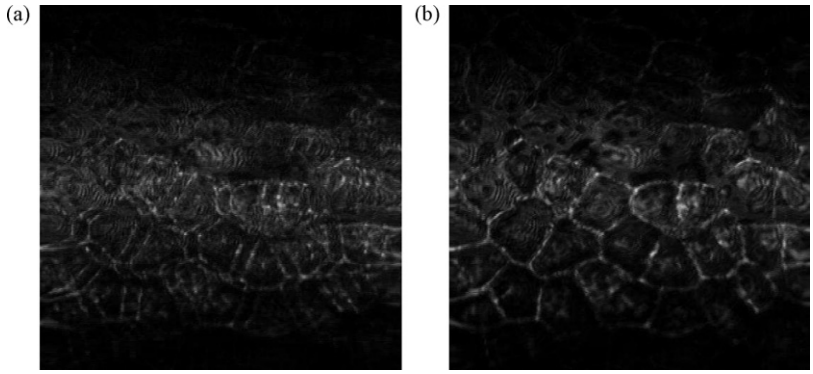

Fig. 4. Effect of pixel delay: before pixel delay correction (a) and after correction (b). Image size: 150 μm.

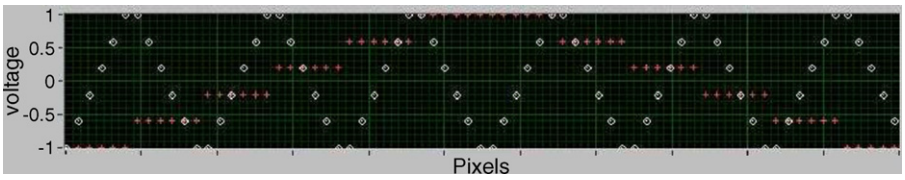

Fig. 5. Bi-direction scanning scheme. White(o): voltage applied onto *X* (fast) axis versus time (pixel sequence); red(+): voltage applied onto *Y* (slow) axis versus time (pixel sequence).The data collecting of each pixel is synchronized with the scan commanding. (For interpretation of the references to color in this figure legend, the reader is referred to the web version of the article.)

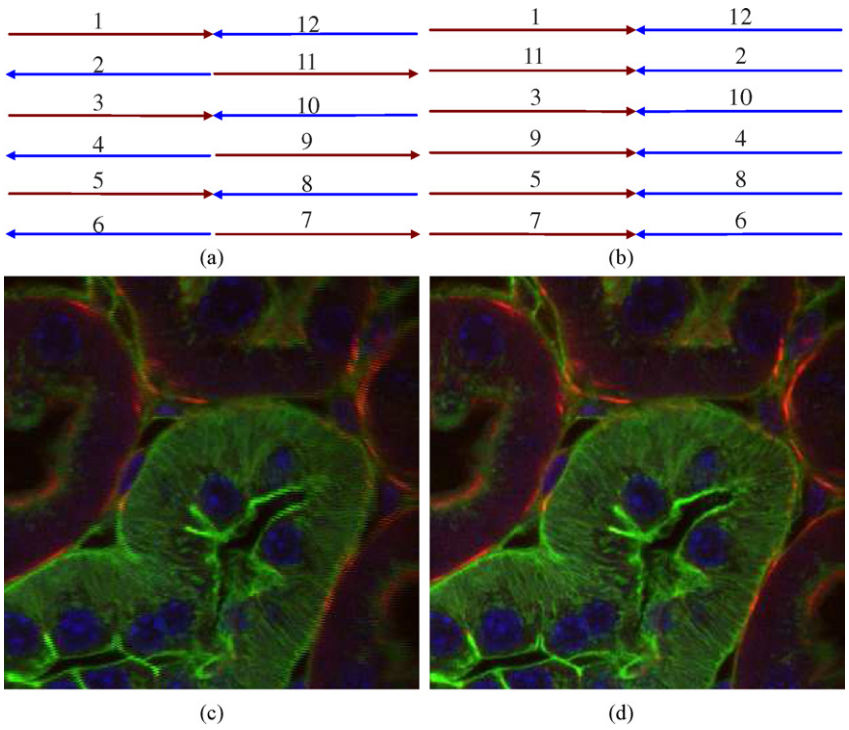

Fig. 6. Interlace line switch scheme: (a) before and (b) after line switch. The brown lines represent the forward scan and the blue lines are the backward scan. The resulting multiphoton image of a mouse kidney is shown in (c) before and (d) after interlace line switch. Image size: 60 μm. (For interpretation of the references to color in this figure legend, the reader is referred to the web version of the article.)

3.3. *Data binning*

As the data acquisition speed can be much higher than the scan command, multiple data acquisition can be performed with data binning to optimize the SNR, as illustrated in Fig. 7. Then, when the image is reconstructed, the software uses simple arithmetic average to bin the data and applies the average value as the intensity of the pixel, as shown in Fig. 8. This method greatly improves the efficient use of the DAQ board and cancels the noise of the image.

In this system, as there are multiple input channels, the acquisition speed of PCI-6251 is 1 MS/s. The galvanometer has a maximum scanning speed limited by the scan angle. To reach an optimal FOV, the galvanometer should work at $\pm 1^{\circ}$, and the maximum scanning speed is ~500 Hz for uni-direction scan with the filling factor of 66%. When the image is collected at speed of 500 × 400 @1 fps, the data collection command is sent at a speed of 800 KS/s. Thus, a 4-point data binning can be performed to match the speed difference between the galvanometer and the data acquisition.

Compared to the algorithm of frame average [5,19], data binning is more robust to the sample drifting, as each pixel are collected at the neighboring time window. Mathematically for instance, for the same digitization speed, one can compare that:

1. For frame average with imaging speed of 500 × 500 @1 fps and average of 4 images, the temporal distance between each averaging pixel is 1 s, therefore the distortion was averaged 1 s away. The advantage for this mode is that for sufficient signal (which is usually not the case when frame averaging or data binning is performed), one can observe the movement of sample drifting from the collected images.
2. For data binning, the same imaging speed requires 2000 × 500 data points in 4 s, and bin every 4 points. Therefore the temporal between each pixel average is 4 μs, 6 orders of magnitude shorter than the frame average.

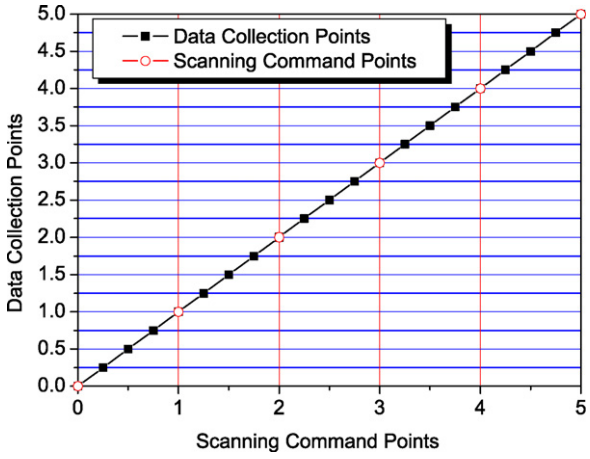

Fig. 7. The mismatch of scanning command speed and data collection speed. The line shows the trace of the galvanometric mirror response.

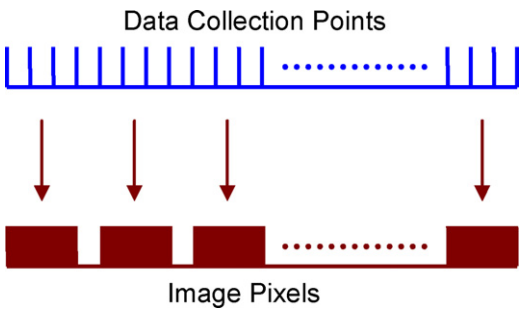

Fig. 8. Schematic diagram of the data binning algorithm.

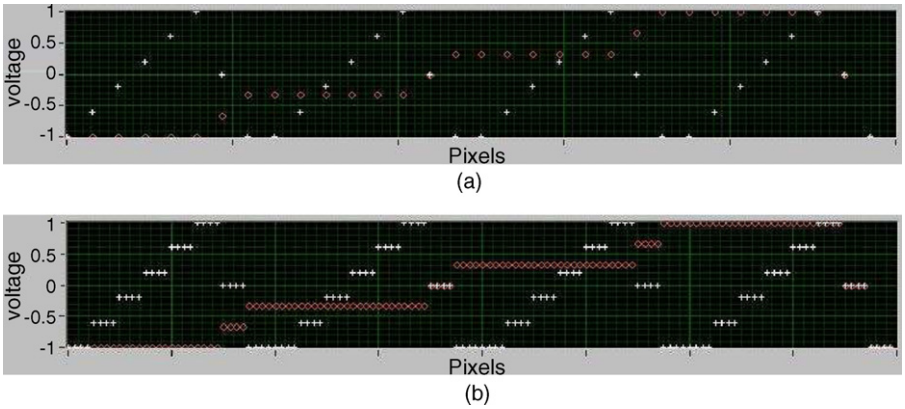

Fig. 9. The controlling schemes of (a) uni-direction scan; (b) uni-direction scan with 4 pixel data binning. White(+): voltage applied onto *X* (fast) axis versus time (pixel sequence); red(o): voltage applied onto *Y* (slow) axis versus time (pixel sequence). The data collecting of each pixel is synchronized with the scan commanding. Image size: 150 μm. (For interpretation of the references to color in this figure legend, the reader is referred to the web version of the article.)

3.4. Region of interest

Usually the image aspect ratio is set to square in order for the visualization and sometimes the requirement of the image processing software (such as several plug-ins in ImageJ). However, to obtain a square image, the scan pixel of the horizontal and vertical pixel should be set separately to count in the filling factor. This is primarily because that the return times for both *X* and *Y* axes are the same, yet it has different filling factors on the image. Also, faster scanning speed can be achieved through the scan on a certain region-of-interest (ROI), thus avoids scanning of the non-interested area [20]. Faster data collection is achieved by reducing the number of *Y* lines collected. As a result, to improve temporal resolution of fast physiological signals, when *X* is set to 512 pixels, single linescan can be repeated at the same *Y* location at 390 fps (data not shown).

3.5. Acquire-On-Fly

In CLSM the scan commanding pixel number and the data collecting pixel number are the same (data binning actually is a mathematical method to sacrifice the image pixel number for a better SNR). However, as the speed of galvanometer and the data acquisition is different, an alternative method to work around this is that only several interval spot is commanded at one speed (could be the fastest speed of the galvanometer), whereas data collection runs at another speed (usually much faster than the galvanometric scan for the data acquisition technique available nowadays). As illustrated in Fig. 7, because the galvanometer's velocity is rather constant when enough interval spot are commanded, an image with increased pixel number can be obtained through remapping the pixels to their respective location sequentially (rather than binning the pixels). The conceptual difference between data binning and AOF lies on that data binning is the increase of data collection speed (Fig. 8), whereas AOF is the decrease of the scanning command speed, relative to the pixel clock.

Fig. 10 demonstrated the effect of employing AOF technique. As shown in Fig. 10, through the application of AOF with a 4× interval pixel sampling between each scan commanding interval, the image sampling frequency can be improved 4 times. Through the adjustment of image aspect ratio accordingly, a square image can be readily collected. Note that in Fig. 10a the horizontal resolution is limited as insufficient pixels are sampled, and the 4× AOF imaging shown in Fig. 10b effectively increased the resolution. Therefore, for different imaging applications, the users have a choice of either acquiring a higher SNR image with data binning, or, obtaining a "larger" image with the AOF technique, depending on the relationships between the SNR, the FOV, and the

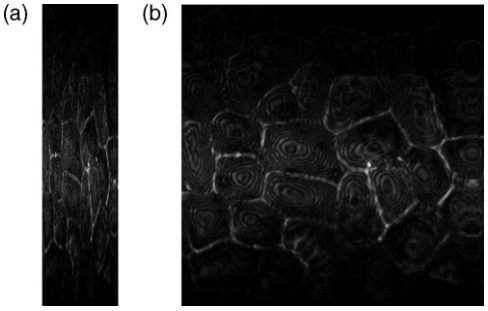

Fig. 10. The confocal images of a bifoliate bush leaf with: (a) the conventional synchronized scanning and sampling mode (pixel number of *X*:Y = 1:4); (b) Acquire-On-Fly mode with 4× sampling speed resulted in a square-frame image with 4× pixel numbers. Image size: 150 μm.

Shannon–Nyquist sampling criteria. For example, if the FOV is set to 100 μm × 100 μm, and the optical resolution is 0.5 μm, then for the optimal resolution (to meet Shannon–Nyquist sampling criteria) we need at least 400 × 400 pixels. We may use the data binning and AOF together to command the galvanometer to run at 100 × 400 @1 fps (where the fast axis runs at only 40K intervals with 400 Hz for uni-directional scan, and filling factor is omitted for simplicity); and collect data at 1600 × 400 @1 fps (where the digitization speed is 640 KS/s). With 4 data binning the SNR is improved; with 4× AOF the image is rescaled to 400 × 400. Of course, the actual resolution is also affected by the SNR of the image so in practice it is always a trade-off between AOF and data binning, for the fixed digitization speed.

4. Conclusions

Galvanometric scanning is the most frequently used laser scanning mechanism in CLSM. Due to the relative low and inconstant speed of the mechanical galvanometric movement, the potential of the confocal system performance is limited. In this work, we analyzed several data acquisition and processing methods, to take fully the advantage of high-speed data acquisition for faster, higher signal-to-noise ratio, and less image distortion data acquisition. Table 1 compared the aspects of the controlling algorithms. The inconstant scanning speed between backward and forward scan in bi-direction scan can lead to image distortion. With interlace line switch the distortion can be completely eliminated. Through the interval pixel reading between two consequent scanning commands, Acquire-On-Fly scan can effectively increase the pixel number and thus the image resolution to match the sampling cri-

Table 1
Features of the algorithms presented in this work.

Algorithm	Image distortion correction	Enhance image collection speed	Improve SNR
Pixel delay	√		
Interlace line switch	√		
Data binning			√
Acquire-On-Fly		√	
Region of interest		√	

teria. The algorithms proposed in this work should be of highly interest to the custom building of a CLSM system, or, to obtain an optimal system performance with current confocal hardware.

Acknowledgements

This research is supported by the National Basic Research Program of China ("973" Program, 2005CB724302), the National Natural Science Foundation of China (60588101, 60808029), the National High Technology Research and Development Program of China ("863" Program, 2008AA030118), and Shanghai Commission of Science and Technology (05DZ22318, 05DZ22325, 064119540, 08PJ14062).

Appendix A.

The software can be downloaded freely from http://biophotonics.sjtu.edu.cn/xipeng/download.htm.

References

[1] J. Pawley, Handbook of Biological Confocal Microscopy, 3rd ed., Springer, Singapore, 2008.
[2] W. Amos, J. White, How the confocal laser scanning microscope entered biological research, Biology of the Cell 95 (6) (2003) 335–342.
[3] J. Conchello, J. Lichtman, Optical sectioning microscopy, Nature Methods 2 (12) (2005) 920–931.
[4] T. Pologruto, B. Sabatini, K. Svoboda, ScanImage: flexible software for operating laser-scanning microscopes, BioMedical Engineering OnLine 2 (1) (2003) 13.
[5] Q. Nguyen, P. Tsai, D. Kleinfeld, MPScope: a versatile software suite for multiphoton microscopy, Journal of Neuroscience Methods 156 (1–2) (2006) 351–359.
[6] P. Xi, B. Rajwa, J. Jones, J. Robinson, The design and construction of a cost-efficient confocal laser scanning microscope, American Journal of Physics 75 (3) (2007) 203–207.
[7] W. Denk, J. Strickler, W. Webb, Two-photon laser scanning fluorescence microscopy, Science 248 (4951) (1990) 73–76.
[8] F. Helmchen, W. Denk, Deep tissue two-photon microscopy, Nature Methods 2 (12) (2005) 932–940.
[9] F. Helmchen, M. Fee, D. Tank, W. Denk, A miniature head-mounted two-photon microscope high-resolution brain imaging in freely moving animals, Neuron 31 (6) (2001) 903–912.
[10] W. Wier, C. Balke, J. Michael, J. Mauban, A custom confocal and two-photon digital laser scanning microscope, American Journal of Physiology-Heart and Circulatory Physiology 278 (6) (2000) H2150–H2156.
[11] A. Majewska, G. Yiu, R. Yuste, A custom-made two-photon microscope and deconvolution system, Pflügers Archiv European Journal of Physiology 441 (2–3) (2000) 398–408.
[12] Q. Nguyen, N. Callamaras, C. Hsieh, I. Parker, Construction of a two-photon microscope for video-rate Ca^{2+} imaging, Cell Calcium 30 (6) (2001) 383–393.
[13] A. Diaspro, G. Chirico, F. Federici, F. Cannone, S. Beretta, M. Robello, Two-photon microscopy and spectroscopy based on a compact confocal scanning head, Journal of Biomedical Optics 6 (3) (2001) 300–310.
[14] G. Nase, P. Helm, T. Reppen, O. Ottersen, A multiphoton laser scanning microscope setup for transcranial in vivo brain imaging on mice, Review of Scientific Instruments 76 (12) (2005) 123702.
[15] P. Xi, Y. Andegeko, L. Weisel, V. Lozovoy, M. Dantus, Greater signal, increased depth, and less photobleaching in two-photon microscopy with 10 fs pulses, Optics Communications 281 (7) (2008) 1841–1849.
[16] P. Xi, Y. Andegeko, D. Pestov, V. Lovozoy, M. Dantus, Two-photon imaging using adaptive phase compensated ultrashort laser pulses, Journal of Biomedical Optics 14 (1) (2009) 014002.
[17] N. Hartell, Simple windows-based software for the control of laser scanning confocal microscopes, Journal of Neuroscience Methods 162 (1–2) (2007) 26–31.
[18] Y. Wu, P. Xi, J. Qu, T. Cheung, M. Yu, Depth-resolved fluorescence spectroscopy reveals layered structure of tissue, Optics Express 12 (14) (2004) 3218–3223.
[19] D. Chou, B. Bower, A. Wax, Low-cost, scalable laser scanning module for real-time reflectance and fluorescence confocal microscopy, Applied Optics 44 (11) (2005) 2013–2018.
[20] V Bansal, S. Patel, P. Saggau, High-speed addressable confocal microscopy for functional imaging of cellular activity, Journal of Biomedical Optics 11 (3) (2006) 034003.